

Defect-Free Axial GaAs/GaAsP Nanowire Quantum Dots with Strong Carrier Confinement

Yunyan Zhang,^{1} Anton V. Velichko,² H. Aruni Fonseka,³ Patrick Parkinson,⁴ George Davis,² James A. Gott,³ Martin Aagesen,⁵ Suguo Huo,⁶ Giorgos Boras,¹ Ana M. Sanchez,³ David Mowbray² and Huiyun Liu^{1*}*

*E-mail: yunyang.zhang.11@ucl.ac.uk; huiyun.liu@ucl.ac.uk

1 Department of Electronic and Electrical Engineering, University College London,
London WC1E 7JE, United Kingdom;

2 Department of Physics and Astronomy, University of Sheffield, Sheffield S3 7RH,
United Kingdom

3 Department of Physics, University of Warwick, Coventry CV4 7AL, United
Kingdom

4 School Department of Physics and Astronomy and the Photon Science Institute,
University of Manchester, M13 9PL, United Kingdom

5 Center for Quantum Devices, Niels Bohr Institute, University of Copenhagen,
Universitetsparken 5, 2100 Copenhagen, Denmark

6 London Centre for Nanotechnology, University College London, London WC1H
0AH, United Kingdom

Abstract:

Defect-free axial quantum dots (QDs) in self-catalysed nanowires (NWs) offer superior compatibility with Si technology and a high degree of structural controllability. However, there has been relatively little optimisation of their structural properties for operation at high temperatures and with long-term stability, particularly in terms of

defect reduction, attainment of deep carrier confinement and incorporation of efficient surface passivation. We report a detailed study of the growth, and structural and optical characterisation of self-catalyzed, defect-free axial GaAsP NWs with deep confinement GaAs QDs. The QDs have very sharp interfaces (1.8~3.6 nm) and dots with very similar structural properties can be closely stacked. High structural quality is maintained when up to 50 QDs are placed in a single NW. The addition of surface passivation layers is shown to be critical in achieving good optical properties, particularly at elevated temperatures. Emission at room temperature, an emission linewidth of <10 meV at 140 K (comparable to the best reported values for all III-V QDs, including nitride ones) and stability of structures stored in an ambient atmosphere for over 6 months are reported. The QDs have the deepest reported carrier confinement (~90 meV) and largest exciton-biexciton splitting (~11 meV) for non-nitride-based III-V NWQDs. These properties indicate the suitability of the structures for devices operating well above liquid-nitrogen temperatures, significantly reducing the operating costs of non-nitride-based III-V NWQD devices.

Key words: nanowire, axially-stacked quantum dots, defect-free crystal, carrier confinement, exciton-biexciton splitting, long-term stability

Introduction

Semiconductor nanowires (NWs) have a unique one-dimensional morphology, which has attracted significant interest, with many potential applications for novel optical emitters.¹⁻³ By changing the axial composition during NW growth, it is possible to

form hetero-structures and introduce one or more quantum structure, for example, quantum dots (QDs), quantum wells (QWs) or superlattices (SLs). QDs provide a unique semiconductor structure with fully quantised electronic states, permitting the fabrication of both high-efficiency classical and non-classical photon emitters. Examples include low threshold current density lasers with reduced sensitivity to temperature variation, trains of regularly spaced single photons, and entangled photon pairs.^{4,5,6} To date, the vast majority of physics and device studies on QDs have utilised self-assembled QDs within planar epitaxial structures, whose formation is strain driven via the Stranski-Krastanov growth mode.⁷ These QDs have a number of significant disadvantages, including: formation at random positions, large inhomogeneous size distributions, limited shape and size control, difficulty in forming stacks of uniform QDs and restrictions on which semiconductors can be combined in a single structure. Formation of dots at pre-determined positions is an essential prerequisite for applications that require either a single, or small, number of QDs.

The growth of QDs within a NW, i.e., a NWQD, is a promising approach for future nano-optoelectronic devices. Unlike self-assembled QDs, QD formation in a NW is not generally strain driven, enabling a greater range of semiconductor material combinations to be used. In addition, the small NW diameter provides high strain tolerance, which permits the combination of materials with large lattice and thermal expansion coefficient mismatch.⁸ The small NW diameter also results in dislocations being unstable, allowing the growth of dislocation-free structures.⁹ The position of the QDs in a NW is fully controlled by the epitaxial growth sequence. Control of both their

shape and size is possible, where the QD diameter is determined by the diameter of the NWs and the height by the epitaxial thickness. Nominally identical QDs can be closely stacked, allowing the formation of molecular systems.¹⁰ Other advantages include growth along the [111]B direction, which should minimise or eliminate exciton splitting^{11,12}, the absence of a wetting layer, and that the NW forms an optical cavity, giving enhanced photon extraction efficiency and directionality.¹¹

NW axial hetero-structures, including QDs, have been studied in a number of systems, e.g. InAsP-InP¹³, GaAs/GaAsP¹⁴ and AlGaAs-GaAs¹⁵. Very narrow spectral linewidths have been reported at low temperatures. A line width of 10 μeV , which is comparable to the best values for self-assembled QDs, has been reported for a GaAs QD in an AlGaAs NW.¹⁵⁻¹⁸ NW QDs have been used to generate both, single photons with extremely low multiphoton probability ($g_2(0) < 0.005$),¹⁹ and polarization entangled photon pairs (via the biexciton–exciton cascading) with fidelities exceeding 80%.^{11,20,21} The majority of previous relevant studies have used NWs fabricated using the Au-catalyzed growth method,^{19,22,23} possibly related to structural control, including sharp QD interfaces and the crystal phases.^{24,25,26} However, NWs catalysed by Au are incompatible with Si-based electronics, and it has been found that Au can be incorporated into GaAs and InAs NWs at levels of the order of 10^{17} – 10^{18} cm^{-3} .^{27,28}

More recently, the non-foreign-metal-catalysed NW growth mode has been developed and applied to produce axial hetero-structures with enhanced properties.²⁹ For example, GaAsSb-based multiple axial superlattices³⁰ and axially stacked InGaAs QDs²⁹ have

demonstrated reduced thresholds for single NW lasers. However, the majority of reports of QD growth still exhibit high-densities of stacking faults, with a mixture of zinc blende (ZB) and wurtzite (WZ) crystal structures,³¹ especially for the widely-used self-catalyzed vapour-liquid-solid growth mode.³² As the ZB and WZ crystal structures have different band gaps, the presence of both polytypes may have a significant impact on the electrical and optical properties of the NW QDs.^{33,34,35} In addition, simulations of GaAs NWs suggest that even well separated twin defects may influence both the optical and electronic properties,³⁶ and calculations for bulk Si has demonstrated carrier scattering by a single twin.³⁷

The self-catalysed growth method utilizes nano-sized group-III metal catalytic droplets that are highly sensitive to the growth environment. Defect-free growth has been reported but for NWs with a diameter in the micrometre range.³⁸ However, full 3D confinement requires the NW diameters to be less than ~100 nm. The sensitivity of the catalytic droplets to their environment increases with reduced droplet size. For example, the Gibbs–Thomson effect,³⁹ makes it challenging to grow structures that are sufficiently small to exhibit true QD behaviour.

In a previous paper, we reported a preliminary demonstration of the growth of a single defect-free axial GaAs inclusion inside self-catalyzed GaAsP nanowires (NWs), with diameters ~50 nm.¹⁴ However, the barrier material had a low P composition (up to 20%) and the emission from the GaAs region did not show features consistent with a QD. In addition, the emission quenched rapidly at low temperatures (~50K); a result of weak

carrier confinement and the absence of any surface passivation. Hence, the suitability of the structures for practical device applications, in particular, stable operation at high temperatures, was not demonstrated. Previously, only nitride NWQDs have consistently demonstrated operation at high temperatures (for example, above liquid nitrogen temperature of 77K). However, nitride materials have a number of limitations. For example, their high growth temperature (commonly $>800\text{ }^{\circ}\text{C}$) can cause damage to other structures and is thus not compatible with many applications. In contrast, non-nitride NWQDs have a much lower growth temperature. However, to date, there have been no detailed reports of stable optical properties above 77K, in particular radiative efficiency and emission linewidth. To improve the operating temperature and carrier confinement, a higher barrier phosphorus composition is required. Efficient surface passivation is also necessary to reduce carrier loss at the NW surface and provide long-term protection of the QDs. In addition, the demonstration of closely spaced, identical QDs, forming molecular-like structures, or arrays of uniform QDs for laser applications, is highly desirable. To date, there has been a lack of reports of detailed studies of defect-free axial QD structures reproducibly grown by self-catalyzed methods.

In this work, we report a investigation of deep carrier confinement, self-catalyzed defect-free GaAs/GaAsP single and multiple axially stacked NWQDs. With robust surface passivation, the QDs exhibit very good optical properties, including narrow emission line widths well above liquid nitrogen temperatures, strong carrier confinement, and a large exciton-biexciton splitting, all beneficial for devices operating at high temperatures.

Results and discussion

GaAsP NWs with phosphorous compositions of 20 or 40% and containing GaAs QDs of varying number and sizes were grown using a flux compensation technique (Supporting information S1). All nanowires had a morphology similar to that shown in the scanning electron microscope (SEM) image of Fig. 1a. It can be seen that the NWs have a highly uniform diameter of 50-60 nm along their entire length. For the single and two QD structures, the QDs are located around the NW mid-point (an example can be seen in the low magnification TEM image and higher magnification inset of the QD in Fig.1a). TEM analysis was carried out for QDs with different sizes. Fig. 1b shows a ~10 nm thick single GaAs QD in a GaAs_{0.8}P_{0.2} NW. The QD has a pure-ZB structure without the presence of any twins. Fig. 1c shows the composition profile along the NW axis for a structure containing a taller, single QD than is shown in Fig.1b. The QD is composed of almost pure GaAs (Although EDX showed that some P was present in the QD, the amount was too low to be accurately quantified). To provide stronger carrier confinement, QDs with higher potential barriers are required. This is achieved by increasing the P content of the GaAsP NW. GaAs QDs with heights ranging from 5-30 nm were grown in GaAs_{0.6}P_{0.4} NWs, all of which were found to exhibit a pure-ZB structure. Figs. 1d-f showing annular dark-field (ADF) images and respective average intensity profiles for ~5, ~10 and ~30 (image only) nm high QDs. The Matthews and Blakeslee limit for relaxation of a planar GaAs layer grown on GaAs_{0.6}P_{0.4} is estimated to be ~15 nm, which is less than the current maximum QD height of 30 nm.⁴⁰ This suggests that the current structures are able to accommodate a relatively high degree of

strain, a consequence of the small cross section of the NWs.

An important requirement for QDs is clearly defined boundaries with sharp interfaces. The interface abruptness should be maximised, especially, for the growth of small height QDs, otherwise the effective height of the QD is increased. The composition profiles shown in Figs. 1d and e demonstrate sharp QD interfaces. The lower (GaAsP-to-GaAs) interface is only ~6 monolayers (\equiv 1.8 nm) wide and the upper (GaAs-to-GaAsP) interface is ~13 monolayers (\equiv 3.6 nm). Both interfaces are significantly more abrupt than those observed in droplet-catalysed NWs where the group-III elements are switched (15-70 nm).^{41,42} To the best of our knowledge, the current interface widths represent the smallest values for defect-free NW QDs where the group-V elements are switched. One reason for the sharp interfaces in the present structures is the low solubility of the group-V elements within the Ga droplet at the high growth temperature of 640 °C (Supporting Information 2).²⁶ The lower interface (growth of GaAs on GaAsP) is slightly sharper than the upper one due to the As/P exchange effect (Supporting Information 3). This is similar to the observation by Priante *et al.* in their heterojunctions grown in self-catalyzed AlGaAs NWs.⁴³ However, the heterojunctions in [43] contain a high-density of stacking faults, which could be a result of uncompensated growth during switching of source fluxes. In contrast, the current interfaces are defect-free.

To investigate if the QD separation affects their structural properties, QD pairs were grown with a small separation of ~10 nm. As seen in Figs. 2a and b these QD pairs are

stacking-fault free, with very similar composition profiles and flat interfaces, indicating that the formation of closely spaced QDs with uniform properties is possible. This provides the potential to form QD molecules or large arrays of closely stacked QDs for laser applications.

To further investigate the suitability of the flux compensation method for the growth of axially-stacked QDs, a sequence of 50 nominally identical GaAs QDs were grown in a GaAs_{0.6}P_{0.4} NW. These QDs appear as white segments in Fig. 2c and d. The NW has a highly uniform diameter of 50 nm along its length and the round Ga droplet is retained at the tip, despite the long NW length of ~12 μm. Both of these observations indicate a highly stable growth environment during the long growth of 1.5 hours. From structural studies on a single representative NW, 65% of the QDs are found to be defect-free (Fig. 1e) and 31% contained a low density of twinning planes (1-4 / dot, as shown in Fig. 2f). Only 4% of the QDs dots (2 dots) were found to have very thin WZ inserts, as shown in Fig. 2g. This demonstrates the growth of a large number of axially stacked QDs with a large percentage (96%) having high structural quality. The twinning typically occurs just above the GaAsP-to-GaAs (first) interface, indicating that the observed defects are formed at the beginning of the QD growth (red arrows in Fig. 2f). This suggests a small droplet size fluctuation at the start of the QD growth due to the flux switching, which should be eliminated by further optimisation of the flux compensation technique. Neighbouring QDs have very similar separations, heights and composition profiles, as shown by composition scans along the NW axis (Figs. 2h and 2i). There is a gradual increase in the QD height and separation from the base to tip of the NW (see Supporting

Information 4).

The emission properties of the QDs were studied by performing micro-photoluminescence (μ -PL) measurements on NWs that were transferred to a Si/SiO₂ substrate. The NW surface forms a thin oxidized layer, which can result in efficient non-radiative carrier recombination.⁴⁴ For GaAs/GaAs_{0.6}P_{0.4} QDs with a bare surface (no passivation layer) only weak QD emission is observed, shown as the black spectrum in Fig. 3. Following surface cleaning in a dilute ammonia solution (NH₄OH:H₂O=1:19) for one minute, stronger but very broad QD emission is observed, blue spectrum in Fig. 3. To improve the optical properties \sim 6 nm GaAs_{0.6}P_{0.4} (to form 3D QD confinement), \sim 18 nm Al_{0.5}Ga_{0.5}As_{0.6}P_{0.4}, and \sim 9 nm GaAs_{0.6}P_{0.4} shell layers were grown radially around the GaAsP core. These layers form a potential barrier to confine carriers within the core region and inhibit them from reaching the NW surface.⁴⁵ The sample with the additional passivation layers, exhibits emission consisting of only a single QD peak at low laser powers, with a narrow linewidth of \sim 500 μ eV. This behaviour is preserved after over 6 months storage in ambient atmosphere (the red spectrum in Fig. 3), demonstrating the importance of the passivation layers for long-term stability. Unless otherwise stated, the measurements described below are for QDs passivated by this method.

The detailed optical emission properties of the QDs were studied by performing μ -PL measurements on surface passivated GaAs_{0.6}P_{0.4} NWs with a core diameter of 50 nm and containing a single GaAs QD of nominal height 25 nm. The QD emission at 6K

consists of a single peak at low laser powers (Fig. 4a). Spectra (Fig. 4a) recorded for different positions along the NW axis show that the emission is highly spatially localized, with an intensity/position profile (inset) determined by the focussed laser spot size ($\sim 1 \mu\text{m}$) and consistent with a small spatially emitting region below the diffraction limit. The majority of NWs exhibit a single, sharp QD emission line at low laser powers although some demonstrate a more complex, slightly red-shifted form, which indicates the presence of defects that are able to perturb the local electronic structure.

With increasing laser power, additional emission lines appear, as shown in Fig. 4b. The inset plots the intensities of the two most spectrally resolved lines as a function of laser power. The different gradients are consistent with exciton and biexciton recombination and the lines demonstrate the expected high power saturation. Their separation is ~ 11 meV which is larger than previously reported values for non-nitride III-V QDs in a NW (for example 6 meV for InAs QDs in GaAs NWs⁴⁶ and 3 meV for GaAsP QDs in GaP NWs).⁴⁷ A large exciton-biexciton separation is beneficial for single photon emission at elevated temperatures.

Fig. 5a shows temperature dependent μ -PL spectra. With increasing temperature, the QD emission broadens; the full width at half maximum (FWHM) is plotted against temperature in Fig. 5b. The solid blue line is a fit to the low temperature (≤ 140 K) data using the function

$$\Gamma(T) = \Gamma_0 + \frac{\Gamma_a}{\exp(E_a / kT) - 1}$$

where Γ_0 is the linewidth at low temperatures (1 meV for the current QD) and Γ_a and

E_a are fitting parameters. This function describes broadening via the scattering of the excitons to a higher energy state by acoustic phonons, with E_a being the energy separation of the two states⁴⁸. The function describes the experimental data well for temperatures up to ~140K (solid blue line in Fig, 5b) and gives a value for E_a of ~3 meV. Simulations performed using nextnano software^{49,50} give confined electron and hole state separations for a 25 nm high and 40 nm diameter QD of ~7 and 1 meV, respectively. Hence, the determined value for E_a is consistent with exciton scattering into an excited QD state. The linewidth at 140K is 9.8 meV. To the best of our knowledge, this is the first report of the emission linewidth at elevated temperatures for a non-nitride NWQD (Supporting information 5), with all previous reports limited to temperatures below ~20K. A linewidth of 9.8 meV is comparable to the lowest published values for nitride NWQDs at elevated temperatures (above ~100K).^{6,51,52} By reducing the QD diameter, and hence increasing the electron and hole confined state separations, it should be possible to achieve smaller line widths at elevated temperatures. For single-photon emission, the exciton and biexciton lines must be spectrally resolvable; this requires their linewidths to be comparable to, or less than, their separation. Thus, the observed separation of 11 meV indicates that single photon emission up to at least 140 K should be possible.

The temperature behaviour of the integrated intensity of a single QD emission exhibits a complex behaviour (Fig. 5c). At low temperatures ($\lesssim 20$ K) a very small activation energy is found. Between 30-70K, the integrated intensity increases with increasing temperature. This can be explained by a change in carrier transport in the GaAsP barrier

material. At low temperatures, carriers are relatively immobile due to localisation caused by alloy fluctuations. As the temperature increases, these carriers are thermally activated from the localisation centres and so a greater number are able to diffuse and be captured by the QD. Hence, there is a region where the QD emission intensity increases with increasing temperature. At high temperatures ($\gtrsim 80\text{K}$) a large activation energy of $\sim 90\text{ meV}$ is found. We have shown from studies of GaAs QWs in GaAsP NWs that both deep electron and hole confinement is achieved, a result of the mixed group-V structure and the large GaAs compressive strain.⁵³ nextnano simulations indicate that the activation energy for electrons is $\sim 30\%$ of the total energy separation of the barrier and QD bandgaps, calculated as 270 meV for the present structure. This suggests an electron activation energy of $\sim 80\text{ meV}$, which is in reasonable agreement with the experimentally determined value of $90\pm 5\text{ meV}$.

Room temperature emission is observable from GaAs QD grown in $\text{GaAs}_{0.6}\text{P}_{0.4}$ NWs and also QDs in NWs with lower P compositions. Fig. 5d shows a sample with a $\text{GaAs}_{0.75}\text{P}_{0.25}/\text{GaAs}$ NWQD and only a 30-nm thick GaAsP passivation layer. The origin of the main emission band is confirmed to be arising from the QD by the spectral mapping shown in the inset of Fig. 5d. High-temperature emission from QDs in a NW is typically observed for wide bandgap and high exciton binding energy materials (Supporting Information S5), e.g. GaN.^{54,55} The observation of emission to relatively high temperatures further confirms the high crystalline, and hence, optical quality of the current QD structures.

In summary, we have demonstrated the growth of deep carrier confinement, defect-free GaAsP NWs containing GaAs QDs of different heights. The QDs have interface widths as low as 6~13 monolayers, allowing the growth of QDs with small heights. It is also possible to form closely separated QD pairs with high uniformity structural properties. The stacking of 50 GaAs QDs in one GaAsP NW is demonstrated, with 96% of the QDs exhibiting high crystalline quality. Surface passivation is shown to be critical for the optical properties of the QDs, particularly at high temperature. The addition of (Al)GaAsP layers results in a significant improvement in the optical properties and results in long-term stability when stored in ambient atmosphere. The passivated QDs have a narrow linewidth of <10 meV at 140K; this is the first report of the high-temperature linewidth for a non-nitride III-V NWQD system, with the value being comparable to the narrowest linewidths reported for nitride-based systems. The QDs exhibit a large carrier confinement energy of ~ 90 meV and emission up to 300K; consistent with a high crystalline quality, deep electron and hole confinement potentials and effective surface passivation. A large exciton-biexciton separation (~ 11 meV) is found. The narrow linewidth, emission at elevated temperatures and large exciton-biexciton separation are all requirements for high temperature operation. Values for the current structures indicate the potential of non-nitride based NWQD quantum emitters to operate well above liquid nitrogen temperatures, this should greatly reduce device-operating costs and significantly increase the range of applications.

Materials and methods

NW growth: The self-catalyzed GaAsP NWs were grown directly on Si(111) substrates by solid-source III–V molecular beam epitaxy. If not otherwise stated, the following growth parameters were used. The core GaAs_{0.6}P_{0.4} (GaAs_{0.8}P_{0.2}) NWs were grown with a Ga beam equivalent pressure, V/III flux ratio, P/(As+P) flux ratio, and substrate temperature of 8.41×10^{-8} Torr, ~30 (40), 41% (12%), and ~640°C, respectively. The GaAs QDs in GaAs_{0.6}P_{0.4} (GaAs_{0.8}P_{0.2}) NWs were grown with a Ga beam equivalent pressure and V/III flux ratio of 8.41×10^{-8} Torr and ~37 (44), respectively. To add passivation shell layers, the Ga droplets were consumed by closing the Ga flux and keeping the group-V fluxes open after the growth of the core. For samples used for optical measurement, GaAsP shells on GaAs_{0.6}P_{0.4} (GaAs_{0.8}P_{0.2}) NWs were then grown with a Ga beam equivalent pressure, V/III flux ratio, P/(As+P) flux ratio, and substrate temperature of 8.41×10^{-8} Torr, 110 (86), 49% (42%), and ~550 °C, respectively. ~18 nm Al_{0.5}Ga_{0.5}As_{0.6}P_{0.4} (to block carriers from reaching the surface), and ~9 nm GaAs_{0.6}P_{0.4} (to protect the AlGaAsP shell) shell layers were grown on the GaAs_{0.6}P_{0.4} core. These layers form a potential barrier to confine carriers within the core region and inhibit them from reaching the NW surface. The Al_{0.5}Ga_{0.5}As_{0.6}P_{0.4} shell was grown with an Al beam equivalent pressure, Ga beam equivalent pressure, V/III flux ratio, P/(As+P) flux ratio, and substrate temperature of 6.33×10^{-8} Torr, 8.41×10^{-8} Torr, 160, 49%, and ~550 °C, respectively. The substrate temperature was measured by a pyrometer.

Scanning Electron Microscope (SEM): The NW morphology was measured with a Zeiss XB 1540 FIB/SEM system.

Transmission electron microscopy (TEM): TEM specimens were prepared by simple mechanical transfer of the nanowires from the as-grown substrate to the holey carbon grid. The TEM measurements were performed with a JEOL 2100 and doubly-corrected ARM200F microscopes, both operating at 200 kV.

Photoluminescence (PL): μ -PL spectra were obtained from single NWs, which had been removed from the original substrate and transferred to a new Si wafer. μ PL spectra of single NWs were excited by a cw 515 nm diode laser. The samples were measured under vacuum inside a continuous flow cryostat (base temperature 6 K). The incident laser was focused with a 20x long working distance microscope objective to a spot size of ~ 1 μ m diameter. The resultant PL was collected by the same microscope objective and focused into a 0.75 m spectrometer, where the spectral components were resolved and detected using a 300 l/mm grating and a nitrogen cooled Si CCD. The spectral resolution was ~ 0.5 meV. Higher resolution measurements were recorded using an 1800 lines/mm grating with a resolution of 0.09 meV.

Room temperature spectra were excited with 280 μ W of 632.8 nm laser light focussed to a spot size of 0.8 μ m diameter. Spectra of 898 individual NWs were recorded and the average of 640, which showed QD emission, used to create the spectrum of Fig. 5d.

Acknowledgements:

The authors acknowledge the support of Leverhulme Trust, EPSRC (grant nos. EP/P000916/1, EP/P000886/1, EP/P006973/1), and EPSRC National Epitaxy Facility. This project has also received funding from the European Union's Horizon 2020 research and innovation programme under the Marie Skłodowska-Curie grant agreement No 721394.

Conflict of interests

The authors declare no competing interests.

Contributions

YZ has written the manuscript, invented the QD growth method and grown all the samples discussed under the supervision of HL. AVV and GD performed μ PL measurements and optical data analysis directed by DM; AVV also performed nextnano simulations. HAF and JAG, performed the TEM and EDX measurements being directed by AMS. DM has performed calculations, general coordination and contributed to the manuscript writing. PP has performed room temperature μ PL measurements and data analysis. SH assisted in the SEM measurement. MA and GB contributed to manuscript discussion. DM, YZ, AVV, HAF and AMS all contributed to multiple revisions and finalising of the manuscript.

Additional information

Supplementary information is available for this paper at <https://doi.org/>

Correspondence and requests for materials should be addressed to Y.Y.Z.

References:

-
1. Zhang, Y., Wu, J., Aagesen, M. & Liu, H. III–V nanowires and nanowire optoelectronic devices. *Journal of Physics D: Applied Physics* **48**, 463001 (2015).
 2. Minot, E.D., Kelkensberg, F., Van Kouwen, M., Van Dam, J.A., Kouwenhoven, L.P., Zwiller, V., Borgström, M.T., Wunnicke, O., Verheijen, M.A. & Bakkers, E.P. Single quantum dot nanowire LEDs. *Nano letters*, **7**, 367-371 (2007).
 3. Reimer, M.E., Bulgarini, G., Akopian, N., Hocevar, M., Bavinck, M.B., Verheijen,

-
- M.A., Bakkers, E.P., Kouwenhoven, L.P. & Zwiller, V. Bright single-photon sources in bottom-up tailored nanowires. *Nature communications*, **3**, 737 (2012).
4. Chen, S., Li, W., Wu, J., Jiang, Q., Tang, M., Shutts, S., Elliott, S.N., Sobiesierski, A., Seeds, A.J., Ross, I. & Smowton, P.M. Electrically pumped continuous-wave III–V quantum dot lasers on silicon. *Nature Photonics* **10**, 307 (2016).
 5. Akopian, N., Lindner, N.H., Poem, E., Berlatzky, Y., Avron, J., Gershoni, D., Gerardot, B.D. & Petroff, P.M. Entangled photon pairs from semiconductor quantum dots. *Physical review letters*, **96**, 130501 (2006).
 6. Holmes, M.J., Choi, K., Kako, S., Arita, M. & Arakawa, Y. Room-temperature triggered single photon emission from a III-nitride site-controlled nanowire quantum dot. *Nano letters*, **14**, 982-986 (2014).
 7. Dubrovskii, V.G., Cirilin, G.E. & Ustinov, V.M. Kinetics of the initial stage of coherent island formation in heteroepitaxial systems. *Physical Review B*, **68**, 075409 (2003).
 8. Ercolani, D., Rossi, F., Li, A., Roddaro, S., Grillo, V., Salviati, G., Beltram, F. & Sorba, L. InAs/InSb nanowire heterostructures grown by chemical beam epitaxy. *Nanotechnology*, **20**, 505605 (2009).
 9. Sanchez, A.M., Zhang, Y., Tait, E.W., Hine, N.D., Liu, H. & Beanland, R. Nonradiative step facets in semiconductor nanowires. *Nano letters*, **17**, 2454-2459 (2017).
 10. Fuhrer, A., Fröberg, L.E., Pedersen, J.N., Larsson, M.W., Wacker, A., Pistol, M.E. & Samuelson, L. Few electron double quantum dots in InAs/InP nanowire heterostructures. *Nano letters*, **7**, 243-246 (2007).
 11. Versteegh, M.A., Reimer, M.E., Jöns, K.D., Dalacu, D., Poole, P.J., Gulinatti, A., Giudice, A. & Zwiller, V. Observation of strongly entangled photon pairs from a nanowire quantum dot. *Nature communications*, **5**, 5298 (2014).
 12. Singh, R. & Bester, G. Nanowire quantum dots as an ideal source of entangled photon pairs. *Physical review letters*, **103**, 063601 (2009).
 13. Haffouz, S., Zeuner, K.D., Dalacu, D., Poole, P.J., Lapointe, J., Poitras, D., Mnaymneh, K., Wu, X., Couillard, M., Korkusinski, M. & Schöll, E. Bright single

-
- InAsP quantum dots at telecom wavelengths in position-controlled InP nanowires: the role of the photonic waveguide. *Nano letters*, **18**, 3047-3052 (2018).
14. Wu, J., Ramsay, A., Sanchez, A., Zhang, Y., Kim, D., Brossard, F., Hu, X., Benamara, M., Ware, M.E., Mazur, Y.I. & Salamo, G.J. Defect-free self-catalyzed GaAs/GaAsP nanowire quantum dots grown on silicon substrate. *Nano letters*, **16**, 504-511 (2015).
 15. Cirlin, G.E., Reznik, R.R., Shtrom, I.V., Khrebtov, A.I., Samsonenko, Y.B., Kukushkin, S.A., Kasama, T., Akopian, N. & Leonardo, L. Hybrid GaAs/AlGaAs Nanowire—Quantum dot System for Single Photon Sources. *Semiconductors*, **52**, 462-464 (2018).
 16. Leandro, L., Gunnarsson, C.P., Reznik, R., Jöns, K.D., Shtrom, I., Khrebtov, A., Kasama, T., Zwiller, V., Cirlin, G. & Akopian, N. Nanowire quantum dots tuned to atomic resonances. *Nano letters*, **18**, 7217-7221 (2018).
 17. Dalacu, D., Poole, P.J. & Williams, R.L. Nanowire-based sources of non-classical light. *Nanotechnology*, **30**, 232001 (2019).
 18. Ates, S., Ulrich, S.M., Ulhaq, A., Reitzenstein, S., Löffler, A., Höfling, S., Forchel, A. & Michler, P. Non-resonant dot–cavity coupling and its potential for resonant single-quantum-dot spectroscopy. *Nature Photonics*, **3**, 724 (2009).
 19. Dalacu, D., Mnaymneh, K., Lapointe, J., Wu, X., Poole, P.J., Bulgarini, G., Zwiller, V. & Reimer, M.E. Ultraclean emission from InAsP quantum dots in defect-free wurtzite InP nanowires. *Nano letters*, **12**, 5919-5923 (2012).
 20. Huber, T., Predojevic, A., Khoshnegar, M., Dalacu, D., Poole, P.J., Majedi, H. & Weihs, G. Polarization entangled photons from quantum dots embedded in nanowires. *Nano Letters*, **14**, 7107-7114 (2014).
 21. Jöns, K.D., Schweickert, L., Versteegh, M.A., Dalacu, D., Poole, P.J., Gulinatti, A., Giudice, A., Zwiller, V. & Reimer, M.E. Bright nanoscale source of deterministic entangled photon pairs violating Bell's inequality. *Scientific reports*, **7**, 1700 (2017).
 22. Reimer, M.E., Bulgarini, G., Fognini, A., Heeres, R.W., Witek, B.J., Versteegh, M.A., Rubino, A., Braun, T., Kamp, M., Höfling, S. & Dalacu, D. Overcoming

-
- power broadening of the quantum dot emission in a pure wurtzite nanowire. *Physical Review B*, **93**, 195316 (2016).
23. van Weert, M.H., Akopian, N., Perinetti, U., van Kouwen, M.P., Algra, R.E., Verheijen, M.A., Bakkers, E.P., Kouwenhoven, L.P. & Zwiller, V. Selective excitation and detection of spin states in a single nanowire quantum dot. *Nano letters*, **9**, 1989-1993 (2009).
- 24) Björk, M.T., Ohlsson, B.J., Sass, T., Persson, A.I., Thelander, C., Magnusson, M.H., Deppert, K., Wallenberg, L.R. & Samuelson, L. One-dimensional heterostructures in semiconductor nanowhiskers. *Applied Physics Letters*, **80**, 1058-1060 (2002).
25. Dick, K.A., Thelander, C., Samuelson, L. & Caroff, P. Crystal phase engineering in single InAs nanowires. *Nano letters*, **10**, 3494-3499 (2010).
26. Dubrovskii, V.G. & Sibirev, N.V. Factors influencing the interfacial abruptness in axial III–V nanowire heterostructures. *Crystal Growth & Design*, **16**, 2019-2023 (2016).
27. Bar-Sadan, M., Barthel, J., Shtrikman, H. & Houben, L. Direct imaging of single Au atoms within GaAs nanowires. *Nano letters*, **12**, 2352-2356 (2012).
28. Perea, D.E., Allen, J.E., May, S.J., Wessels, B.W., Seidman, D.N. & Lauhon, L.J. Three-dimensional nanoscale composition mapping of semiconductor nanowires. *Nano letters*, **6**, 181-185 (2006).
29. Tatebayashi, J., Kako, S., Ho, J., Ota, Y., Iwamoto, S. & Arakawa, Y. Room-temperature lasing in a single nanowire with quantum dots. *Nature Photonics*, **9**, 501 (2015).
30. Ren, D., Ahtapodov, L., Nilsen, J.S., Yang, J., Gustafsson, A., Huh, J., Conibeer, G.J., Van Helvoort, A.T., Fimland, B.O. & Weman, H. Single-mode near-infrared lasing in a GaAsSb-based nanowire superlattice at room temperature. *Nano letters*, **18**, 2304-2310 (2018).
31. Priante, G., Patriarche, G., Oehler, F., Glas, F. & Harmand, J.C. Abrupt GaP/GaAs interfaces in self-catalyzed nanowires. *Nano letters*, **15**, 6036-6041 (2015).

-
32. Zhang, Y., Aagesen, M., Holm, J.V., Jørgensen, H.I., Wu, J. & Liu, H. Self-catalyzed GaAsP nanowires grown on silicon substrates by solid-source molecular beam epitaxy. *Nano letters*, **13**, 3897-3902 (2013).
 33. Loitsch, B., Winnerl, J., Grimaldi, G., Wierzbowski, J., Rudolph, D., Morkötter, S., Döblinger, M., Abstreiter, G., Koblmüller, G. & Finley, J.J. Crystal phase quantum dots in the ultrathin core of GaAs–AlGaAs core–shell nanowires. *Nano letters*, **15**, 7544-7551 (2015).
 34. Bouwes Bavinck, M., Jöns, K.D., Zieliński, M., Patriarche, G., Harmand, J.C., Akopian, N. & Zwiller, V. Photon cascade from a single crystal phase nanowire quantum dot. *Nano letters*, **16**, 1081-1085 (2016).
 35. Akopian, N., Patriarche, G., Liu, L., Harmand, J.C. & Zwiller, V. Crystal phase quantum dots. *Nano letters*, **10**, 1198-1201 (2010).
 36. Shimamura, K., Yuan, Z., Shimojo, F. & Nakano, A. Effects of twins on the electronic properties of GaAs. *Applied Physics Letters*, **103**, 022105 (2013).
 37. Forouhi, A.R. & Bloomer, I. Optical properties of crystalline semiconductors and dielectrics. *Physical review B*, **38**, 1865 (1988).
 38. Zhang, G., Takiguchi, M., Tateno, K., Tawara, T., Notomi, M., & Gotoh, H. Telecom-band lasing in single InP/InAs heterostructure nanowires at room temperature. *Science Advances*, **5**, eaat8896 (2019).
 39. Zhang, Y., Sanchez, A.M., Sun, Y., Wu, J., Aagesen, M., Huo, S., Kim, D., Jurczak, P., Xu, X. & Liu, H. Influence of droplet size on the growth of self-catalyzed ternary GaAsP nanowires. *Nano letters*, **16**, 1237-1243 (2016).
 40. Fitzgerald, E.A. Dislocations in strained-layer epitaxy: theory, experiment, and applications. *Materials science reports*, **7**, 87-142 (1991).
 41. Ouattara, L., Mikkelsen, A., Sköld, N., Eriksson, J., Knaapen, T., Čavar, E., Seifert, W., Samuelson, L. & Lundgren, E. GaAs/AlGaAs nanowire heterostructures studied by scanning tunneling microscopy. *Nano letters*, **7**, 2859-2864 (2007).
 42. Cornet, D.M. & LaPierre, R.R. InGaAs/InP core–shell and axial heterostructure nanowires. *Nanotechnology*, **18**, 385305 (2007).

-
43. Priante, G., Glas, F., Patriarche, G., Pantzas, K., Oehler, F. & Harmand, J.C. Sharpening the interfaces of axial heterostructures in self-catalyzed AlGaAs nanowires: experiment and theory. *Nano letters*, **16**, 1917-1924 (2016)
44. Joyce, H.J., Baig, S.A., Parkinson, P., Davies, C.L., Boland, J.L., Tan, H.H., Jagadish, C., Herz, L.M. & Johnston, M.B. The influence of surfaces on the transient terahertz conductivity and electron mobility of GaAs nanowires. *Journal of Physics D: Applied Physics*, **50**, 224001 (2017).
45. Jiang, N., Parkinson, P., Gao, Q., Breuer, S., Tan, H.H., Wong-Leung, J. & Jagadish, C. Long minority carrier lifetime in Au-catalyzed GaAs/Al_xGa_{1-x}As core-shell nanowires. *Applied Physics Letters*, **101**, 023111 (2012).
46. Tatebayashi, J., Ota, Y., Ishida, S., Nishioka, M., Iwamoto, S. & Arakawa, Y. Site-controlled formation of InAs/GaAs quantum-dot-in-nanowires for single photon emitters. *Applied Physics Letters*, **100**, 263101 (2012).
47. Borgström, M.T., Zwiller, V., Müller, E. & Imamoglu, A. Optically bright quantum dots in single nanowires. *Nano letters*, **5**, 1439-1443 (2005).
48. Gammon, D., Snow, E. S., Shanabrook, B. V., Katzer, D. S., & Park, D. Homogeneous Linewidths in the Optical Spectrum of a Single Gallium Arsenide Quantum Dot. *Science*, **273**, 87-90 (1996).
49. Fonseka, H.A., Velichko, A.V., Zhang, Y., Gott, J.A., Davis, G.D., Beanland, R., Liu, H., Mowbray, D.J. and Sanchez, A.M. Self-formed Quantum Wires and Dots in GaAsP-GaAsP Core-Shell Nanowires. *Nano letters*, **19**, 4158-4165 (2019)
50. Birner, S., Zibold, T., Andlauer, T., Kubis, T., Sabathil, M., Trellakis, A., Vogl, P. Nextnano: general purpose 3-D simulations. *IEEE Transactions on Electron Devices*, **54**, 2137-2142 (2007).
51. Deshpande, S., Das, A. & Bhattacharya, P. Blue single photon emission up to 200 K from an InGaN quantum dot in AlGaN nanowire. *Applied Physics Letters*, **102**, 161114 (2013).

-
52. Deshpande, S. & Bhattacharya, P. An electrically driven quantum dot-in-nanowire visible single photon source operating up to 150 K. *Applied Physics Letters*, **103**, 241117 (2013).
 53. Zhang, Y., Davis, G., Fonseka, H.A., Velichko, A., Gustafsson, A., Godde, T., Saxena, D., Aagesen, M., Parkinson, P.W., Gott, J.A. & Huo, S. Highly Strained III–V–V Coaxial Nanowire Quantum Wells with Strong Carrier Confinement. *ACS nano*. **13**, 5931–5938 (2019).
 54. Tribu, A., Sallen, G., Aichele, T., Andre, R., Poizat, J.P., Bougerol, C., Tatarenko, S. & Kheng, K. A high-temperature single-photon source from nanowire quantum dots. *Nano letters*, **8**, 4326-4329 (2008).
 55. Ostapenko, I.A., Hönig, G., Rodt, S., Schliwa, A., Hoffmann, A., Bimberg, D., Dachner, M.R., Richter, M., Knorr, A., Kako, S. & Arakawa, Y. Exciton acoustic-phonon coupling in single GaN/AlN quantum dots. *Physical Review B*, **85**, 081303 (2012).

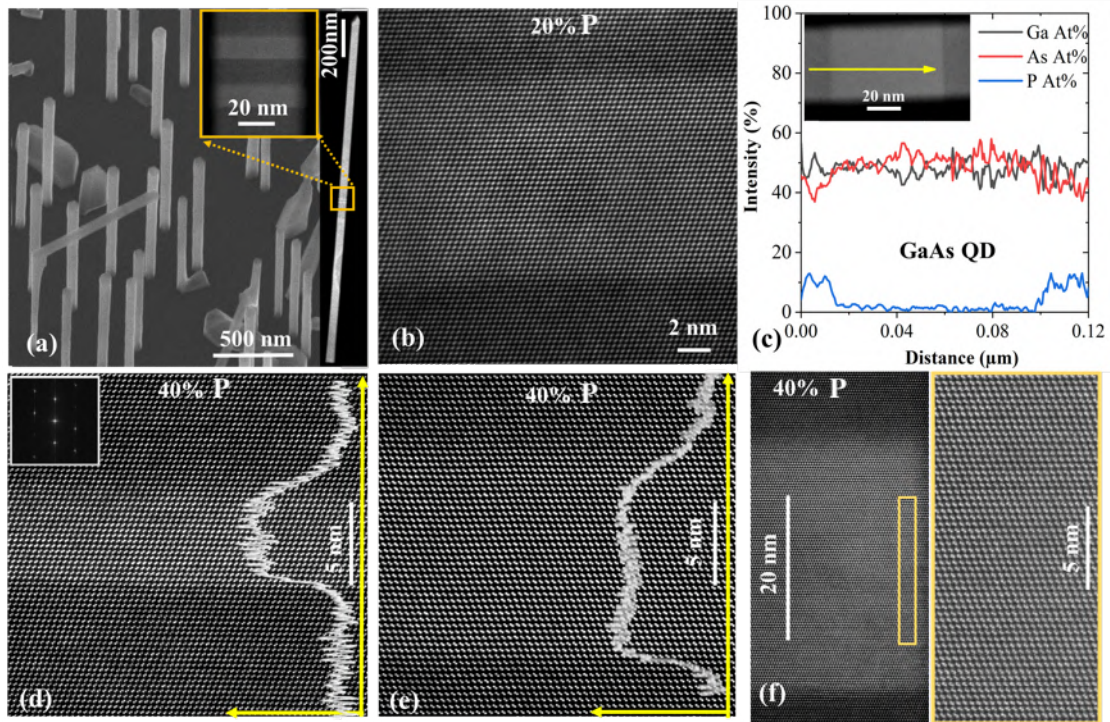


Fig. 1 Morphology and crystalline quality of GaAsP NWs with defect-free GaAs QDs. a 30°-tilted SEM image of GaAs_{0.6}P_{0.4} NWs with two GaAs QDs located around the mid-point of the NW (see inset). **b** High-magnification, ADF image of a ~10 nm-high GaAs QD within a GaAs_{0.8}P_{0.2}NW. **c** EDX composition profile along the axis of the GaAs_{0.8}P_{0.2}/GaAs QD shown in the inset. Annular ADF images of **d** ~5-nm-high, **e** ~10-nm-high and **f** ~30-nm-high GaAs QDs in GaAs_{0.6}P_{0.4} NWs. The overlay curves in **(d)** and **(e)** are the integrated ADF intensity profiles. The inset in **(d)** is the SAED pattern for the region around the QD.

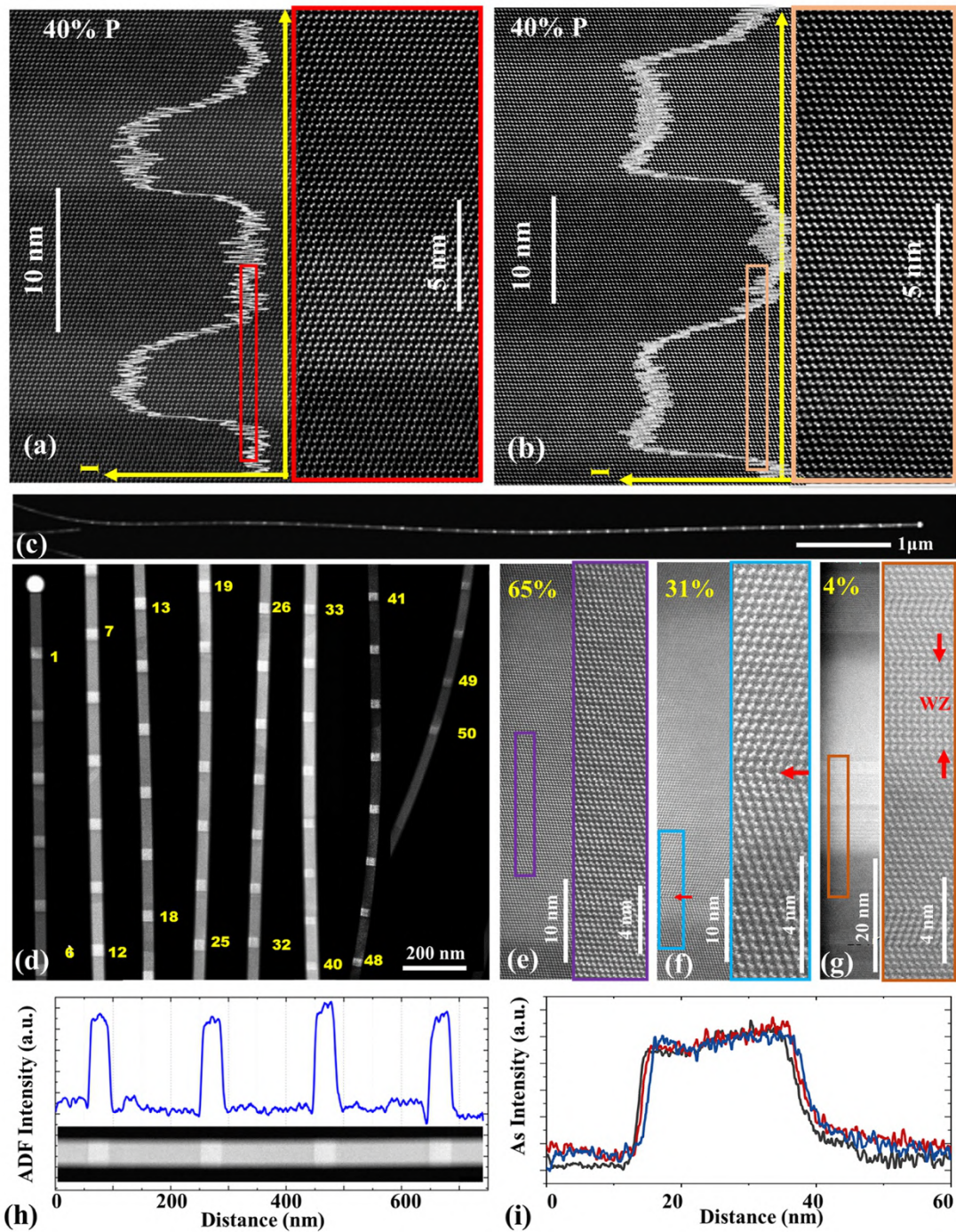


Fig. 2 Structural properties of axially-stacked GaAs_{0.6}P_{0.4} / GaAs QDs. **a** and **b** Low-magnification (left) and high-magnification (right) ADF images of 5-nm-high and 10-nm-high closely-stacked pairs of QDs. The overlay curves are the integrated ADF intensity profiles. **c** and **d** low-magnification ADF images of the entire NW containing 50 QDs. High-

magnification ADF images of representative QDs **e**, without a defect, **f** with one twin plane, and **g** containing WZ segments, as indicated by the red arrows. **h** axial integrated intensity profiles of the NW segment shown in the inset. **i** As composition profiles for three adjacent QDs from the lower region of the NW.

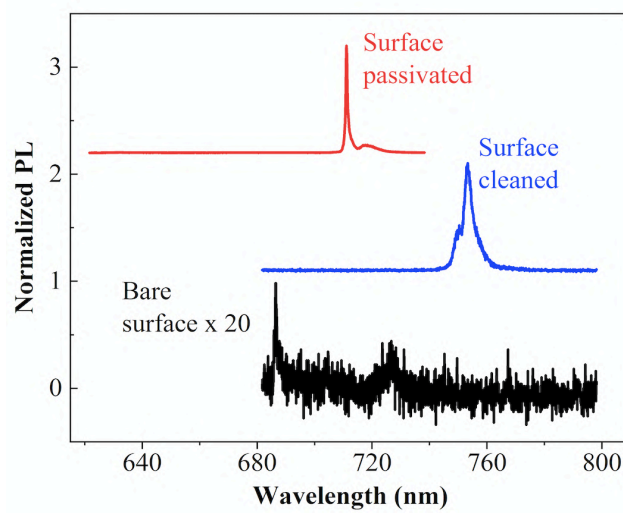


Fig 3. μ -PL spectra of a GaAs QDs in GaAsP NW with an unpassivated surface (black), without surface passivation but with surface cleaning using an ammonia solution (blue), and with surface-passivation layers (red).

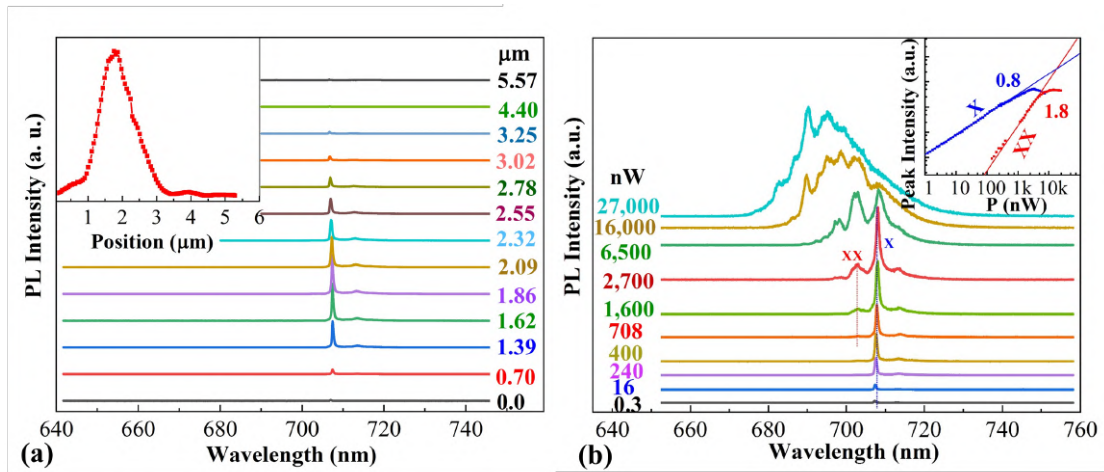


Fig 4. Optical properties of a surface-passivated single ~25 nm GaAs dot in a ~50 nm diameter GaAs_{0.6}P_{0.4} NW at 6K. a Position-dependent μ-PL spectra along the length of a NW. The laser power is 50 nW. The inset plots the intensity of the QD emission against exciting laser position. **b** Power-dependent μ-PL spectra. The inset plots the intensities of two of the emission lines, X and XX, against laser power.

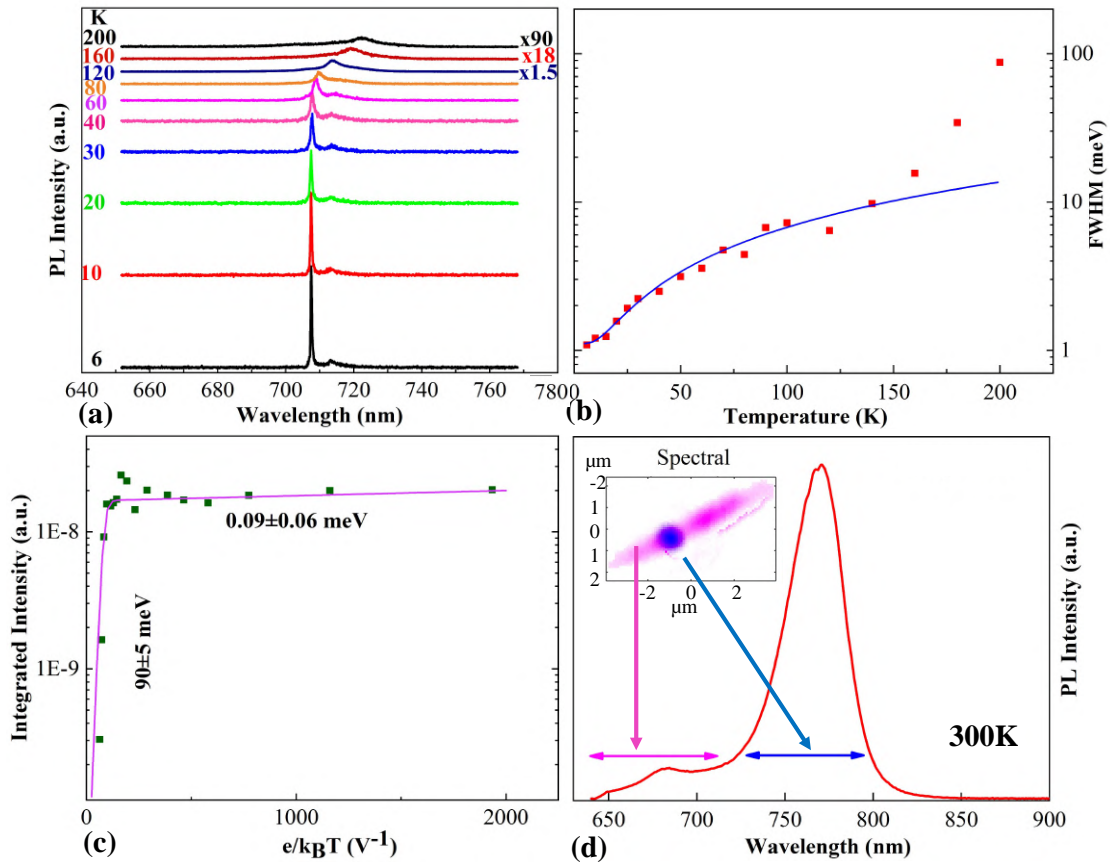


Fig 5. QD temperature-dependent emission properties. **a** Temperature-dependent μ PL spectra of a surface-passivated GaAs_{0.6}P_{0.4}/GaAs QD. **b** QD emission linewidth and **c** integrated PL intensity plotted against temperature. The solid blue line in (b) is a fit to the low temperature data. **d** PL spectrum at 300K created by combining spectra recorded separately from 640 individual GaAs_{0.75}P_{0.25} NWs each containing a single GaAs dot. The insets show a spectral map image of a representative NW, with two spectral bands used to create the image as indicated by the horizontal arrows in the main part of the figure.

Supporting Information

Structural and Optical Properties of Defect-Free Axial GaAs/GaAsP Nanowire Quantum Dots with Strong Carrier Confinement

Yunyan Zhang,^{1} Anton V. Velichko,² H. Aruni Fonseka,³ Patrick Parkinson,⁴ George Davis,² James A. Gott,³ Martin Aagesen,⁵ Suguo Huo,⁶ Giorgos Boras,¹ Ana M. Sanchez,³ David Mowbray² and Huiyun Liu^{1*}*

*E-mail: yunyang.zhang.11@ucl.ac.uk; huiyun.liu@ucl.ac.uk

1 Department of Electronic and Electrical Engineering, University College London, London WC1E 7JE, United Kingdom;

2 Department of Physics and Astronomy, University of Sheffield, Sheffield S3 7RH, United Kingdom

3 Department of Physics, University of Warwick, Coventry CV4 7AL, United Kingdom

4 School Department of Physics and Astronomy and the Photon Science Institute, University of Manchester, M13 9PL, United Kingdom

5 Center for Quantum Devices, Niels Bohr Institute, University of Copenhagen, Universitetsparken 5, 2100 Copenhagen, Denmark

6 London Centre for Nanotechnology, University College London, London WC1H 0AH, United Kingdom

S1. Flux-compensation growth method

To determine the factors leading to the formation of stacking faults, a comparison was made between two types of Ga-catalyzed GaAsP NWs that are formed during the growth of a single sample. These were formed within significantly different densities, and hence separation of both the NWs and clusters formed by parasitic growth between NWs. Type-I NWs are shown in Fig. S1a. They exhibit a highly uniform diameter (50~60 nm) along their entire length (3~4

μm), except very close to their base and tip where the diameter decreases. Type-II NWs are shown in Fig. S1b and exhibit a noticeable tapering, with a gradually reduced diameter from the base towards the tip, indicating a decreasing droplet size during growth. Type-I NWs commonly have a pure ZB crystal structure except close to the tip and base. In contrast, the type-II NWs typically have a high density of stacking faults along their entire length. This suggests that the reduction of the droplet size correlates with the formation of stacking faults. It is found that the stacking faults at the base and tip of the NWs are generated by an unstable droplet at the start and end of the growth, when the source flux beams are switched on and off.

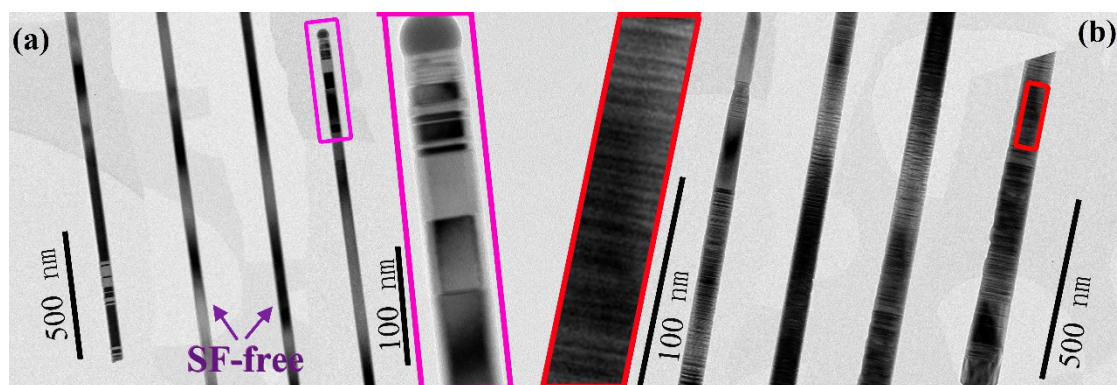


Fig. S1 | Relationship between droplet size fluctuation and the formation of stacking faults.

Transmission electron microscopy (TEM) images of GaAsP NWs with **a** highly uniform diameters and **b** a gradually reducing diameter from base to tip. The dark and sharp transverse lines are stacking faults.

To grow high quality axial hetero-structures with sharp interfaces, rapid switching of the growth fluxes is required. However, these flux switches have to be performed very carefully to avoid fluctuations of the droplet size, and hence the formation of stacking faults, and the potential formation of WZ segments.^{1,2,3} To avoid these fluctuations when growing axial hetero-structures, it is crucial to maintain the droplet super-saturation, which is achieved using a “flux compensation” method. When the P flux is turned off/on, the As flux has to increase/decrease accordingly, with the change in As flux volume proportional to that of the P flux volume. Our previous studies have shown that the P nucleation is stronger than that of

As,⁴ so the compensating As flux should be larger than that of the P flux change. By varying the ratio (As flux change) : (P flux change) for the growth of a number of samples, with P compositions of either 20 or 40%, we have determined the optimum value to be between 1.48 and 1.80, with the precise value depending on the NW density, inter-NW parasitic growth density, growth temperature and III-V ratio. QDs grown outside this optimum compensation range tend to have a high-density of stacking faults. Fig. S2 shows TEM images obtained from GaAs QDs grown in GaAs_{0.8}P_{0.2} NWs using a compensation ratio of 2.2. As this compensation ratio is outside the optimum compensation range, the QDs of different heights (10~50 nm) contain a high-density of stacking faults; in contrast to the high quality, defect-free QDs grown within the optimum compensation range. This comparison clearly demonstrates the potential of the flux compensation technique and that its use is critical in obtaining high quality QDs.

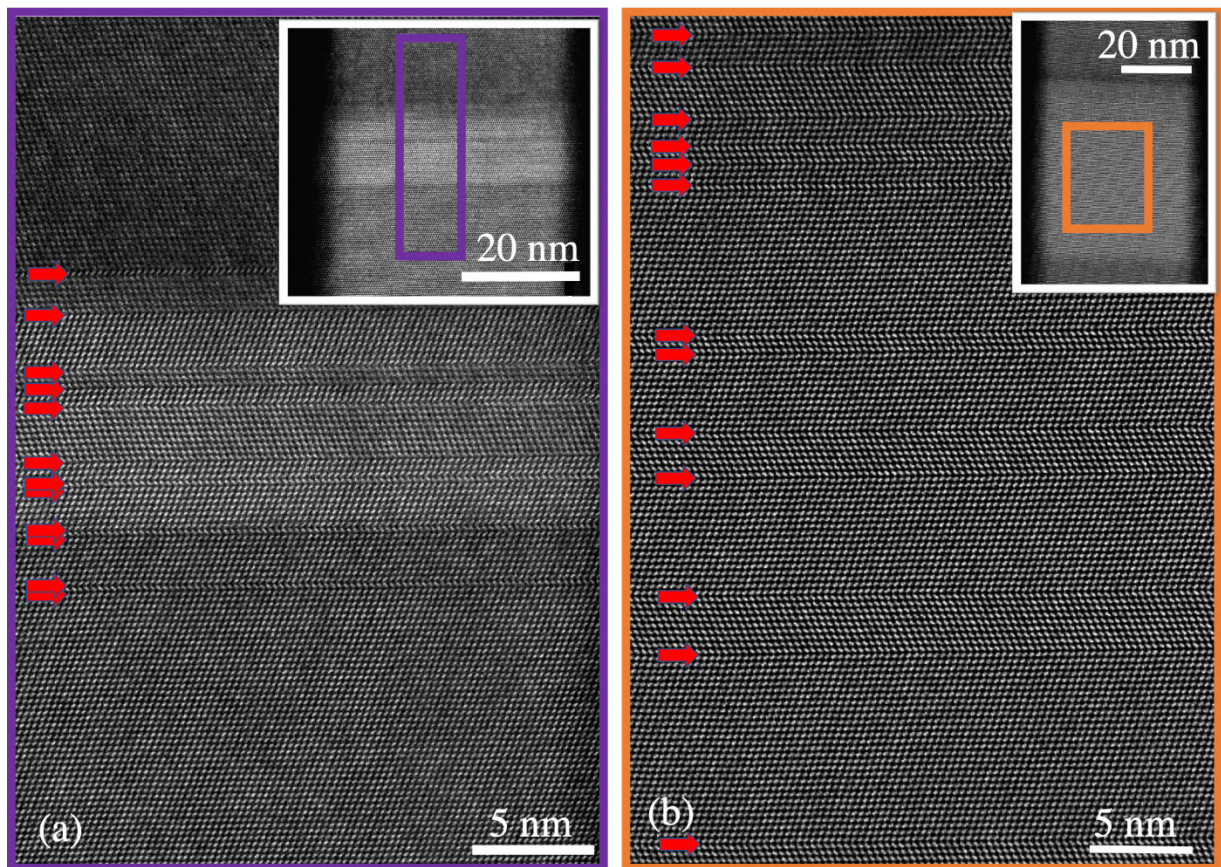


Fig. S2. STEM images of GaAs QDs grown in GaAs_{0.8}P_{0.2} NWs with a compensation ratio of 2.2. The QD height is ~10 nm in **a** and ~50 nm in **b**. The red arrows show the locations of twins. The insets are

low-magnification TEM images of the NW segments containing the QDs.

S2. Reduced reservoir effect for As and P in Ga metal droplets

The high solubility of group-III metals in the metal droplets used by the VLS method results in a significant reservoir effect; this can prevent the fabrication of sharp hetero-interfaces, especially interfaces that rely on a significant depletion of one element.⁵ In contrast, group-V elements have a much lower solubility in the liquid metal compared to group-III metals, especially at high growth temperatures. This allows for a very fast material depletion and switching.⁶ The current GaAsP NW growth is performed at a relatively high temperature of 640 °C. This minimises the reservoir effect for As and P, resulting in the formation of sharp hetero-interfaces and the growth of almost pure GaAs QDs (Fig. 1c, main paper).

S3. Asymmetrical GaAs/GaAsP hetero interfaces

During compositional switching, As/P inter-diffusion occurs, reducing the sharpness of the interface. P atoms are more strongly bonded to Ga atoms, hence it is more difficult to replace P atoms with As atoms.⁷ As a result, inter-diffusion at the GaAsP-to-GaAs interface is weaker than at the GaAs-to-GaAsP interface, leading to the former interface being sharper.

S4. Variation in QD size and separation along the NW axis

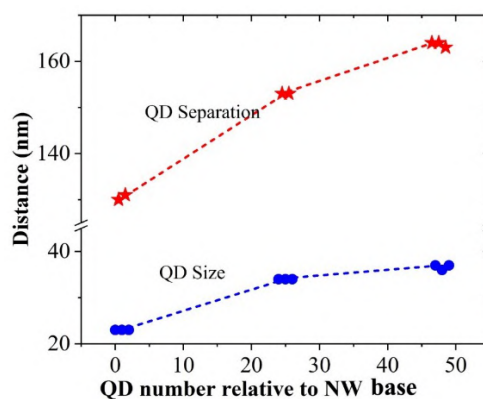


Fig. S3. Variation in QD size and separation along the NW axis.

There is an increase in both the QD height and QD separation from the base to tip of the NW (Fig. S3), which suggests a gradual environment change in source material collection. By gradually reducing the QD growth time during the NW growth it should be possible to achieve uniform QDs along the entire NW, as required for laser applications.

S5. Summary of published NWQD emission linewidths as a function of temperature

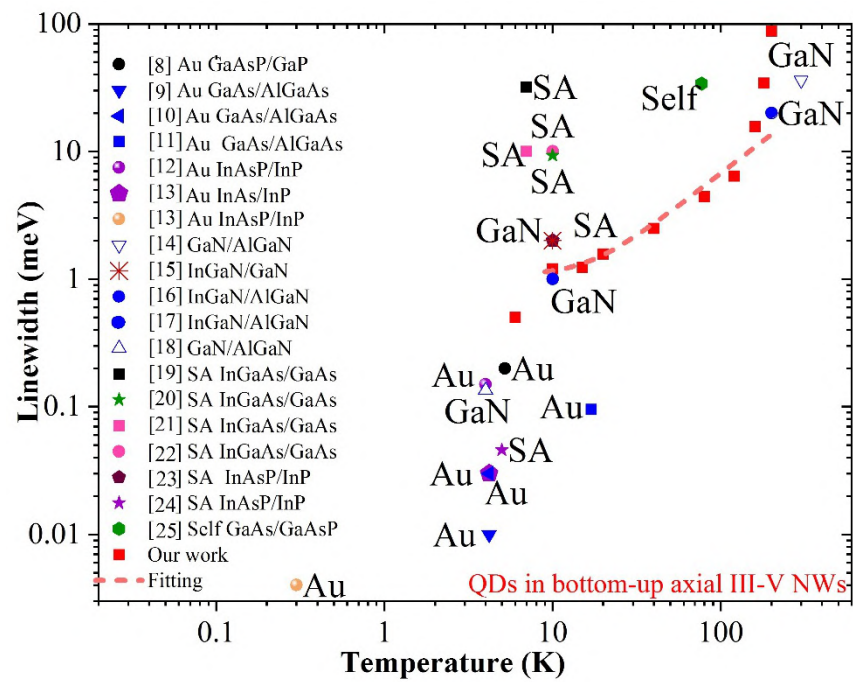


Fig. S4. Emission linewidth summary for axial III-V QDs grown by bottom-up methods. The pink dash line is the fit to our temperature dependent data (Fig. 5b). “SA” indicates selective-area growth. “Au” indicates Au catalysed growth and “GaN” indicates gallium nitride-based NWs.

Table S1. Emission linewidth summary for various III-V NWQD systems

1st Author	NW type	Material system	T (K)	Linewidth (meV)
Bottom-up III-V QDs				
Borgstrom ⁸	Au	GaAsP/GaP	5.2	0.2
Cirlin ⁹	Au	GaAs/AlGaAs	4.2	0.01
Leandro ¹⁰	Au	GaAs/AlGaAs	4.2	0.03
Heinrich ¹¹	Au	GaAs/AlGaAs	17.0	0.095
Haffouz ¹²	Au	InAsP/InP	4.0	0.15
Dalacu ¹³	Au	InAs/InP	4.2	0.03

Reimer ¹⁴	Au	InAsP/InP	0.3	0.004
Holmes ¹⁵	Nitride	GaN/AlGaN	300.0	36.0
Deshpande ¹⁶	Nitride	InGaN/GaN	10.0	2.0
Deshpande ¹⁷	Nitride	InGaN/AlGaN	10 & 200	1-2 & 15-20
Holmes ¹⁸	Nitride	GaN/AlGaN	4.0	0.135
Tatebayashi ¹⁹	SA	InGaAs/GaAs	7.0	32.0
Tatebayashi ²⁰	SA	InGaAs/GaAs	10.0	9.3
Tatebayashi ²¹	SA	InGaAs/GaAs	7.0	10.0
Tatebayashi ²²	SA	InGaAs/GaAs	10.0	10
Yanase ²³	SA	InAsP/InP	10.0	2.0
Dorenbos ²⁴	SA	InAsP/InP	5.0	0.046
Wu ²⁵	Self-catalyzed	GaAs/GaAsP	77.0	34
Our work	Self-catalyzed	GaAs/GaAsP	6.0	0.5
Our work	Self-catalyzed	GaAs/GaAsP	140.0	9.8
Other QDs in III-V NWs				
Bavinck ²⁶	Crysal Phase	InP	4.2	0.023
Kremer ²⁷	top-down	InGaAs/GaAs	4.5	0.045
Munsch ²⁸	top-down	InAs/GaAs	4.2	0.004
Francaviglia ²⁹	radial	GaAs/AlGaAs	12.0	0.74
Heiss ³⁰	radial	GaAs/AlGaAs	4.2	0.029
Shang ³¹	radial	GaAs/AlAs	4.2	0.037
Weib ³²	radial	GaAs/AlGaAs	5.0	1.0
Yan ³³	radial	GaAs/InP	5.5	1.28
Yu ³⁴	radial	GaAs/AlGaAs	4.2	0.1

Fig. S4 and Table S1 summarize previous reports of emission linewidths for different III-V QDNW systems. The current work represents the first report of narrow emission linewidths for non-nitride based NWQDs above 20K. High-temperature emission from QDs in a NW is typically observed for systems with a wide bandgap and large exciton binding energy, e.g. GaN. Despite a much smaller band gap and exciton binding energy, we observe emission at 140K with a linewidth of 9.8 meV. This value is comparable with the best-reported values for nitride NWQDs.

1.Priante, G., Patriarche, G., Oehler, F., Glas, F. & Harmand, J.C. Abrupt GaP/GaAs interfaces in self-catalyzed nanowires. *Nano letters*, **15**, 6036-6041 (2015).

-
2. Verheijen, M.A., Immink, G., de Smet, T., Borgström, M.T. & Bakkers, E.P. Growth kinetics of heterostructured GaP–GaAs nanowires. *Journal of the American Chemical Society*, **128**, 1353-1359 (2006).
 3. Todorovic, J., Kauko, H., Ahtapodov, L., Moses, A.F., Olk, P., Dheeraj, D.L., Fimland, B.O., Weman, H. & Van Helvoort, A.T.J. The effects of Sb concentration variation on the optical properties of GaAsSb/GaAs heterostructured nanowires. *Semiconductor Science and Technology*, **28**, 115004 (2013).
 4. Zhang, Y., Aagesen, M., Holm, J.V., Jørgensen, H.I., Wu, J. & Liu, H. Self-catalyzed GaAsP nanowires grown on silicon substrates by solid-source molecular beam epitaxy. *Nano letters*, **13**, 3897-3902 (2013).
 5. Li, N., Tan, T. Y. & Gösele, U. Transition region width of nanowire hetero- and pn-junctions grown using vapor–liquid–solid processes. *Appl. Phys. A: Mater. Sci. Process* **90**, 591-596 (2008).
 6. Björk, M. T., Ohlsson, B. J., Sass, T., Persson, A. I., Thelander, C., Magnusson, M. H. & Samuelson, L. One-dimensional steeplechase for electrons realized. *Nano Lett.* **2**, 87–89 (2002).
 7. Decobert, J. & Patriarche, G. Transmission electron microscopy study of the InP/InGaAs and InGaAs/InP heterointerfaces grown by metalorganic vapor-phase epitaxy. *Journal of Applied Physics*, **92**, 5749-5755 (2002).
 8. Borgström, M.T., Zwiller, V., Müller, E. & Imamoglu, A. Optically bright quantum dots in single nanowires. *Nano letters*, **5**, 1439-1443 (2005).
 9. Cirlin, G.E., Reznik, R.R., Shtrom, I.V., Khrebtov, A.I., Samsonenko, Y.B., Kukushkin, S.A., Kasama, T., Akopian, N. & Leonardo, L. Hybrid GaAs/AlGaAs Nanowire—Quantum dot System for Single Photon Sources. *Semiconductors*, **52**, 462-464 (2018).
 10. Leandro, L., Gunnarsson, C.P., Reznik, R., Jöns, K.D., Shtrom, I., Khrebtov, A., Kasama, T., Zwiller, V., Cirlin, G. & Akopian, N. Nanowire quantum dots tuned to atomic resonances. *Nano letters*, **18**, 7217-7221 (2018).
 11. Heinrich, J., Huggenberger, A., Heindel, T., Reitzenstein, S., Höfling, S., Worschech, L. & Forchel, A. Single photon emission from positioned GaAs/AlGaAs photonic nanowires. *Applied Physics Letters*, **96**, 211117 (2010).
 12. Haffouz, S., Zeuner, K.D., Dalacu, D., Poole, P.J., Lapointe, J., Poitras, D., Mnaymneh, K., Wu, X., Couillard, M., Korkusinski, M. & Schöll, E. Bright single InAsP quantum dots at telecom wavelengths in position-controlled InP nanowires: the role of the photonic

-
- waveguide. *Nano letters*, **18**, 3047-3052 (2018).
13. Dalacu, D., Mnaymneh, K., Lapointe, J., Wu, X., Poole, P.J., Bulgarini, G., Zwiller, V. & Reimer, M.E. Ultraclean emission from InAsP quantum dots in defect-free wurtzite InP nanowires. *Nano letters*, **12**, 5919-5923 (2012).
 14. Reimer, M.E., Bulgarini, G., Fognini, A., Heeres, R.W., Witek, B.J., Versteegh, M.A., Rubino, A., Braun, T., Kamp, M., Höfling, S. & Dalacu, D. Overcoming power broadening of the quantum dot emission in a pure wurtzite nanowire. *Physical Review B*, **93**, 195316 (2016).
 15. Holmes, M.J., Choi, K., Kako, S., Arita, M. & Arakawa, Y. Room-temperature triggered single photon emission from a III-nitride site-controlled nanowire quantum dot. *Nano letters*, **14**, 982-986 (2014).
 16. Deshpande, S., Heo, J., Das, A. & Bhattacharya, P. Electrically driven polarized single-photon emission from an InGaN quantum dot in a GaN nanowire. *Nature communications*, **4**, 1675 (2013).
 17. Deshpande, S., Das, A. & Bhattacharya, P. Blue single photon emission up to 200 K from an InGaN quantum dot in AlGaIn nanowire. *Applied Physics Letters*, **102**, 161114 (2013).
 18. Holmes, M., Kako, S., Choi, K., Arita, M. & Arakawa, Y. Spectral diffusion and its influence on the emission linewidths of site-controlled GaN nanowire quantum dots. *Physical Review B*, **92**, 115447 (2015).
 19. Tatebayashi, J., Kako, S., Ho, J., Ota, Y., Iwamoto, S. & Arakawa, Y. Room-temperature lasing in a single nanowire with quantum dots. *Nature Photonics*, **9**, 501 (2015).
 20. Tatebayashi, J., Ota, Y., Ishida, S., Nishioka, M., Iwamoto, S. & Arakawa, Y. Highly uniform, multi-stacked InGaAs/GaAs quantum dots embedded in a GaAs nanowire. *Applied Physics Letters*, **105**, 103104 (2014).
 21. Tatebayashi, J. & Arakawa, Y. Lasing in a single nanowire with quantum dots. In *Quantum Dots and Nanostructures: Growth, Characterization, and Modeling XIV, International Society for Optics and Photonics* **10114**, 1011406 (February, 2017).
 22. Tatebayashi, J. & Arakawa, Y. Recent progress in nanowire quantum-dot lasers. In *Quantum Dots and Nanostructures: Growth, Characterization, and Modeling XV, International Society for Optics and Photonics* **10543**, 1054303 (2018, February).

-
23. Yanase, S., Sasakura, H., Hara, S. & Motohisa, J. Single-photon emission from InAsP quantum dots embedded in density-controlled InP nanowires. *Japanese Journal of Applied Physics*, **56**, 04CP04 (2017).
 24. Dorenbos, S.N., Sasakura, H., Van Kouwen, M.P., Akopian, N., Adachi, S., Namekata, N., Jo, M., Motohisa, J., Kobayashi, Y., Tomioka, K. & Fukui, T. Position controlled nanowires for infrared single photon emission. *Applied Physics Letters*, **97**, 171106 (2010).
 25. Wu, J., Ramsay, A., Sanchez, A., Zhang, Y., Kim, D., Brossard, F., Hu, X., Benamara, M., Ware, M.E., Mazur, Y.I. & Salamo, G.J. Defect-free self-catalyzed GaAs/GaAsP nanowire quantum dots grown on silicon substrate. *Nano letters*, **16**, 504-511 (2015).
 26. Bouwes Bavinck, M., Jöns, K.D., Zieliński, M., Patriarche, G., Harmand, J.C., Akopian, N. & Zwiller, V. Photon cascade from a single crystal phase nanowire quantum dot. *Nano letters*, **16**, 1081-1085 (2016).
 27. Kremer, P.E., Dada, A.C., Kumar, P., Ma, Y., Kumar, S., Clarke, E. & Gerardot, B.D. Strain-tunable quantum dot embedded in a nanowire antenna. *Physical Review B*, **90**, 201408 (2014).
 28. Munsch, M., Kuhlmann, A.V., Cadeddu, D., Gérard, J.M., Claudon, J., Poggio, M. & Warburton, R.J. Resonant driving of a single photon emitter embedded in a mechanical oscillator. *Nature communications*, **8**, 76 (2017).
 29. Francaviglia, L., Giunto, A., Kim, W., Romero-Gomez, P., Vukajlovic-Plestina, J., Friedl, M., Potts, H., Güniat, L., Tütüncüoğlu, G. & Fontcuberta i Morral, A. Anisotropic-Strain-Induced Band Gap Engineering in Nanowire-Based Quantum Dots. *Nano letters*, **18**, 2393-2401 (2018).
 30. Heiss, M., Fontana, Y., Gustafsson, A., Wüst, G., Magen, C., O'regan, D.D., Luo, J.W., Ketterer, B., Conesa-Boj, S., Kuhlmann, A.V. & Houel, J. Self-assembled quantum dots in a nanowire system for quantum photonics. *Nature materials*, **12**, 439 (2013).
 31. Shang, X., Yu, Y., Zha, G., Li, M., Wang, L., Xu, J., Ni, H. & Niu, Z. Small linewidth and short lifetime of emission from GaAs/AlAs core/shell quantum dots on the facet of GaAs nanowire. *Journal of Physics D: Applied Physics*, **46**, 405102 (2013).
 32. Weiß, M., Kinzel, J.B., Schüle, F.J., Heigl, M., Rudolph, D., Morkötter, S., Döblinger, M., Bichler, M., Abstreiter, G., Finley, J.J. & Koblmüller, G. Dynamic acoustic control of individual optically active quantum dot-like emission centers in heterostructure nanowires. *Nano letters*, **14**, 2256-2264 (2014).
 33. Yan, X., Tang, F., Wu, Y., Li, B., Zhang, X. & Ren, X. Growth of isolated InAs quantum

dots on core-shell GaAs/InP nanowire sidewalls by MOCVD. *Journal of Crystal Growth*, **468**, 185-187 (2017).

34. Yu, Y., Zha, G.W., Shang, X.J., Yang, S., Sun, B.Q., Ni, H.Q. & Niu, Z.C. Self-assembled semiconductor quantum dots decorating the facets of GaAs nanowire for single-photon emission. *National Science Review*, **4**, 196-209 (2016).